Journal of Visualization, Vol. 11, No. 2 (2008)163-172

Regular Paper

Visualization of a Rotating Flow under Large-Deformed Free Surface Using Anisotropic Flakes

Tasaka, Y.*[1], Ito, K.*[2] and Iima, M.*[3]

*1 Graduate School of Engineering, Hokkaido University, N13W8, Sapporo, 060-8628, Japan.
E-mail: tasaka@eng.hokudai.ac.jp
*2 Graduate School of Science, Hokkaido University, N10W8, Sapporo, 060-0810, Japan.
*3 Research Institute for Electronic Science, Hokkaido University, N12W6, Sapporo, 060-0812, Japan.

Received 20 March 2007
Revise 25 December 2007

Abstract : This study aims to clarify the relationship between the deformation of a free surface and flow transition in a "switching phenomenon" process. In a flow driven by a rotating disk in a cylindrical open vessel, the free surface irregularly changes its shape from axisymmetric to nonaxisymmetric and vice versa with repeating up-and-down motion (so-called "switching phenomenon"). The flow under the free surface was visualized by anisotropic flakes. When the free surface assumes a parabolic shape, the flow is distinguished by three regions; local circulation region, rigid vortex region and meridional circulation region. The flow transition in the switching phenomenon was shown by snapshots and movies of the visualized flow; the flow near the free surface is laminar even if the shape of the free surface changes to nonaxisymmetric during the time at which the free surface attaches to the bottom of the vessel. After the free surface detaches from the disk, the flow near the free surface becomes turbulent. When the free surface changes to axisymmetric while descending to the bottom, the flow changes from turbulent to laminar flow and the local circulation region reemerges at the center of the vessel.

Keywords : Rotating flow, Free surface, Flow transition, Visualization, Anisotropic flakes.

1. Introduction

Rotating flows accompanied with a free surface are important in geo- science and also in non-linear dynamics in fluids; the flow and the shape of the free surface are interesting. A simplest setup is the free-surface flow in a stationary cylinder driven by the endwall rotation. Even at a low rotation speed, where the free surface deformation is negligible, symmetry breaking of the axisymmetric flow (Lopez, et al., 2001) and polygonal shape with rotating core in the flow (Poncet and Chauve, 2007), has been observed. A large-deformed free surface under a high-speed rotation causes further interesting phenomena including the rotating polygonal shape of the free surface (Jansson et al., 2006). Suzuki et al. (2006) reported the temporally-irregular switching of the free surface at a rotation speed corresponding to the laminar- turbulent transition, $Re \sim 10^5$ (Reed and Saric, 1989). The region of the Reynolds number where the switching phenomenon occurs is located between the region in which the shape of the free surface is axisymmetric and the region in which the shape is nonaxisymmetric. During the switching process, the typical depth of the free surface greatly changes as well as the axisymmetry of the free surface. A temporal change of the surface shape under the constant rotation has been reported for the polygon shapes (Jansson et al., 2006) and the flow driven by a smaller disk at a higher Reynolds number (Vatistas, 1990), however, because the Reynolds numbers are too high

or too low, the surface changes can not be related to the laminar-turbulent transition. Suzuki et al. (2006) suggested that the mechanism of the switching is the decrease/increase of the pressure in the central region caused by the change of the flow characteristics, i.e., the laminar-turbulent transition. However, the flow pattern has not been studied yet. In this paper, by means of flow visualization, we study the structure of the flow in a cylinder driven by the endwall, and clarify that the switching process is directly related to the laminar- turbulent transition.

2. Experimental Method

Figure 1 shows the coordinate system and a schematic illustration of the experimental setup; an open end cylinder filled with fluid, a disk-type rotor and a magnetic stirrer. The disk-type rotor in the glass vessel is driven by rotating magnetic field generated by the magnetic stirrer (AS-ONE, HPS-500R) beneath the vessel. The disk rotor was made by using a disk-type magnetic stirring bar (AS-ONE); its radius is slightly smaller than the inner radius of the cylinder (R = 42.5 mm) to reduce friction at the side wall. The estimated gap between the cylinder and the rotor is $\Delta R = 0.5$ mm. The top of the rotor was covered with a glass plate, and hence we regard the top of the rotor as the bottom of the vessel. Rotation of the disk follows the rotation of the magnetic field in the magnetic stirrer.

Tap water was filled into the vessel with height $H = 40$ mm at rest, and then the aspect ratio is $\Gamma = H/R = 0.941$. The disk-type rotor generates a rotational flow. The relevant parameters for this experimental system are at least four: Reynolds number, Froude number, Weber number and aspect ratio. The shape of the surface deformation is governed by the Froude number defined by an appropriate characteristic flow speed. In surface switching, the surface deformation shows a non-periodic switching between two different shapes, which suggests that the characteristic flow speed changes due to a flow transition. To examine the effect of the laminar - turbulent transition suggested by Suzuki et al. (2006), we use the Reynolds number to describe the result. However, we note that the Froude number also changes as the rotation speed changes. Reynolds number of the flow is defined as $Re \equiv 2\pi\Omega R^2/\nu$ (Ω is the rotating speed of the rotor and ν is the kinematic viscosity of water). Rotating speed of the rotor was varied from $\Omega = 328$ rpm to $\Omega = 1015$ rpm; these rotations correspond to the range of the Reynolds number from $Re = 0.62 \times 10^5$ to $Re = 1.92 \times 10^5$. In the range of the Reynolds number, as shown in Fig. 2, a temporally averaged height of the free surface at the center of the vessel, $\langle h \rangle$, decreases with respect to Re and it becomes zero around $Re = 1.0 \times 10^5$. The switching phenomenon can be observed at $Re \sim 1.3 \times 10^5$. Kalliroscope flakes, AQ-1000 rheoscopic concentration, were used to visualize the fluid motion. It is a suspension of microscopic crystalline platelets (the main ingredient of the platelet is guanine, which has 1.62 g/cm^3 in density, and the size of the platelet is $6 \times 30 \times 0.07$ μm), these platelets are arranged parallel to the planes of shear flow. Large scale fluid motion at the vertical cross section along the center line of the cylinder can be

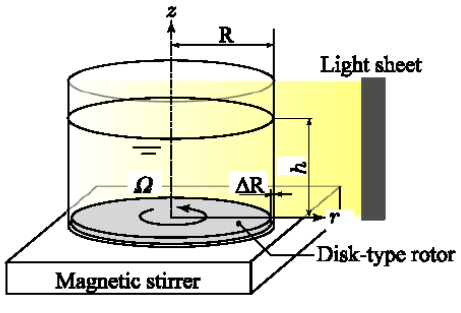

Fig. 1. Experimental setup; the disk-type rotor in the glass vessel is driven by a rotating magnetic field generated by the magnetic stirrer beneath the vessel.

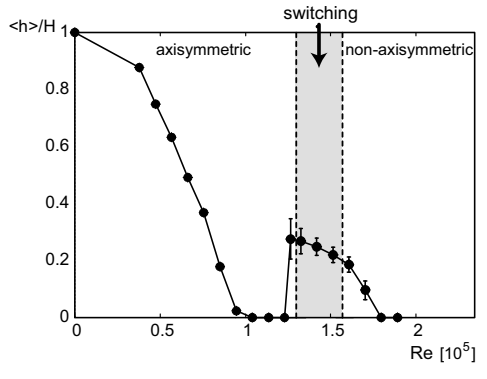

Fig. 2. Variation of a temporally averaged height of the free surface at the center of the vessel with respect to Reynolds number.

visualized by using an incident light sheet (150 W Halogen lamp and cylindrical lens were used in this study). This provides contrast of brightness information as reported before by Park et al. (1981) and Thoroddsen et al. (1999). Note that the main aim of visualization is detect qualitative changes of vortex structures which do not depend on the detailed position of the light. Snapshots of the visualized flow were taken by a digital camera (Nikon, D1X) to observe the flow pattern under the large-deformed free surface; movies of the flow were recorded by a high speed video camera (Photron, FASTCAM-Max 120K) to investigate a temporal variation of the flow pattern. Shutter speed in both measurements was set at 1/2000 sec and the frame rate of the movie was 2000 fps.

3. Results and Discussions

3.1 Flow Pattern and Shape of the Free Surface

Figure 3 shows photographs of the flow visualized by Kalliroscope at each speed of the disk rotation; large-scale shear flow at the vertical cross section along the center line of the cylinder is expressed by contrast of the brightness. Figure 3(a) is stationary liquid in the vessel; there is no typical pattern of the brightness because of random orientation of the Kalliroscope flakes.

As the disk rotation speed increases, the free surface between the liquid and surrounding air changes its form from flat to an inverted-bell shape. This is to balance the centrifugal force and the pressure gradient on the radial direction. Figure 3(b) shows the flow under the free surface, where the rotation speed of the disk is Ω = 328 rpm (Re = 0.62 × 10^5). The thin boundary layer (called Ekman layer) exists on the rotating disk and the vertical scale of the Ekman layer is $l_E = [\nu/(2\pi\Omega)]^{1/2}$ ~ 0.2 mm, but it is not observed. Three regions between the center line and the side wall of the vessel can be observed; (A) local circulation region ($0 < r < 0.2$R), (B) rigid vortex region (0.2R $< r < 0.5$R) and (C) meridional circulation region ($r > 0.5$R) (see Fig. 3(d)). Kalliroscope flakes are arranged along the direction of the maximum principal strain of the flow. There are high brightness streaks in the region (A) and it shows local circulation in the meridional direction. Such circulation is also observed for smaller Reynolds numbers (Leopz et al., 2004). These streaks form the boundary of the regions. In the region (B), there is no typical strain pattern, therefore the flow can be regarded as fully laminar. Calculation of the radius of the rigid vortex in the Appendix shows a consistent result for the distinction of the rigid vortex region. The region (C) has the meridional circulation as expressed by the streaks. Near-bottom flow induced by centrifugal force at the bottom of the vessel produces centrifugal flow near the bottom, which causes the meridional circulation. As expressed with brightness distribution, the meridional circulation is typically enhanced near the deformed free surface, like Taylor vortex appearing in the flow between coaxial two cylinders. Small-scale turbulent motion is superimposed to the large-scale circulation.

As the disk rotation increases, deformation of the free surface increases, finally, it attaches to the bottom of the vessel (Fig. 3(c), Reynolds number and the rotation speed are Re = 1.13 × 10^5 and Ω = 600 rpm, respectively). The local circulation region disappears but the rigid vortex region remains between the free surface and the meridional circulation region. The fluid near the center is circularly hollowed by the attached free surface, hence there is no transmission of the momentum from the

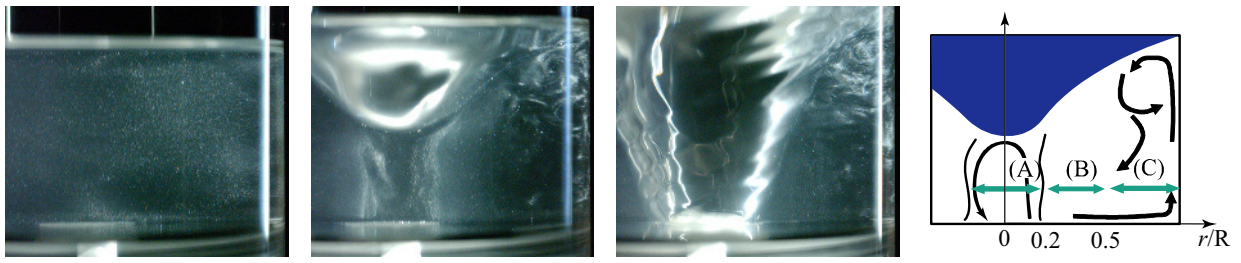

(a) (b) (c) (d)

Fig. 3. Visualized photographs; (a) state of rest, (b) Re = 0.62 × 10^5 (Ω = 328 rpm) and (c) Re = 1.13 × 10^5 (Ω = 600 rpm). (d) Schematic of three regions under the axisymmetric free surface; (A) local circulation region, (B) rigid vortex region and (C) meridional circulation region.

rotating disk to the fluid. The meridional circulation becomes clear and is localized near the free surface. There is instability due to shear between both layers on the free surface, but it is out the focus of this study and here we have no further discussion about it.

At a higher disk rotation speed, the switching phenomenon explained in the introduction can be observed, namely, the free surface attached to the bottom changes from axisymmetric shape to nonaxisymmetric shape with two humps (Fig. 4(a)), then the free surface ascends detaching from the bottom of the vessel (Figs. 4(b) and (c)). The typical switching loop is shown in Figs. 5(a)-(e); the top view (above) and the side view (bottom) of the shape of the free surface. The photographs in Fig. 4 show typical form of the free surface and the flow under the free surface in the switching process, where the Reynolds number and the rotation speed are $Re = 1.46 \times 10^5$ and $\Omega = 770$ rpm, respectively. Schematics attached to each figure show the form of the free surface observed from above and the observation angle. The flow structure between the free surface and the side wall of the vessel, the rigid vortex region and the meridional circulation region, still remains while the free surface is attached to the bottom (Fig. 4(a)). It becomes wholly turbulence after the free surface detaches from the bottom (Figs. 4(b) and (c)); this turbulent flow remains while the free surface repeats its up-and-down motion. This turbulent flow may be caused by the rupture of the axial symmetry, and the appearance of a strong shear flow between the free surface and the rotating disk. The oscillating free surface above the bottom reattaches to the bottom when the surface shape reverts to axisymmetric. At this time, the flow also reverts to the distinguished two regions as shown in Fig. 4(a). We observed the switching between the laminar flow and the turbulent flow during the switching of the surface shape.

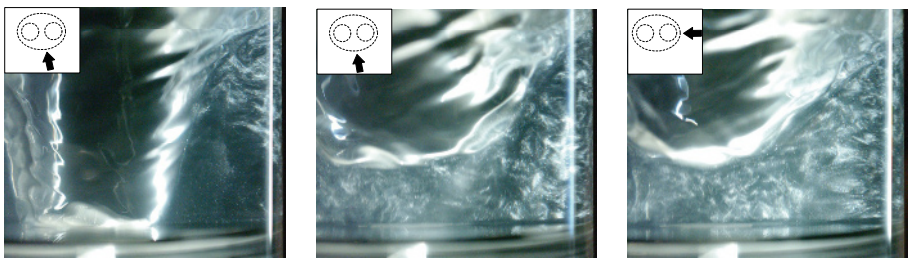

(a) (b) (c)

Fig. 4. Visualized photographs taken at $Re = 1.46 \times 10^5$ ($\Omega = 770$ rpm); (a) the free surface has nonaxisymmetric shape but is still attached to the bottom, (b) and (c) the deformed free surface detaches from the bottom of the vessel. Schematics attached to each figure show the form of the free surface observed from above and the observation angle.

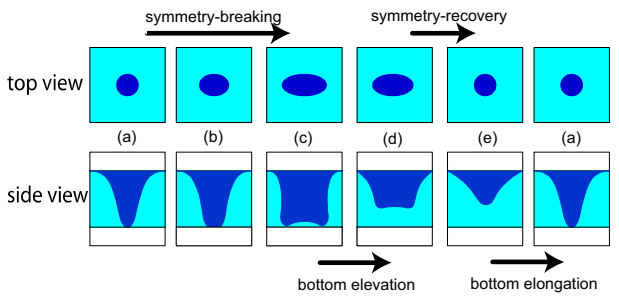

Fig. 5. Variation of the shape of the free surface during the switching phenomenon; top view (above) and side view (bottom). The free surface repeats its deformation from (a) to (e).

When the rotation speed increases beyond that of the switching state, the free surface does not attach to the bottom of the vessel and its position is kept around a certain height (Fig. 6, $Re = 1.65 \times 10^5$ and $\Omega = 870$ rpm). In this condition, the flow is wholly turbulent and there is large-scale circulation near the bottom. The height of the free surface decreases with increasing rotation speed, and finally the free surface attaches to the bottom while keeping a nonaxisymmetric shape.

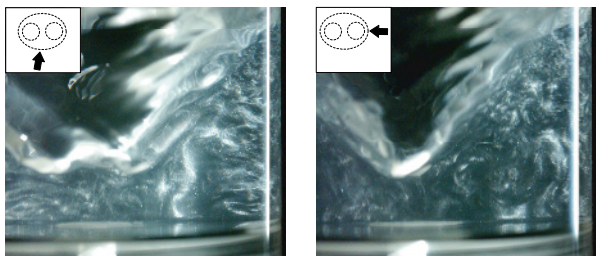

(a) (b)

Fig. 6. Visualized photographs taken at Re = 1.65 × 10^5 (Ω = 870 rpm). Schematics attached to each figure show the form of the free surface observed from above and the observation angle.

3.2 Temporal Variations of the Flow Patterns

Figure 7(a) shows a snapshot extracted from a movie of the visualized flow taken by the high speed video camera. Reynolds number and the speed of the disk rotation are Re = 0.62 × 10^5 and Ω = 330 rpm. The condition of the experiment is the same with that in Fig. 3(b), thus the flow pattern observed in the figure, which is distinguished by three regions, corresponds to that observed in Fig. 3(b). Figure 7(b) is a temporal variation of a line image extracted from the frames of the movie at r/ R = 0.58. The time length of the image is 0.2 sec and the extracted line image has 1 pixel in width. The line image expresses the temporal variation of the flow, however, there is no typical pattern in the image because the flow under the free surface is quasi steady.

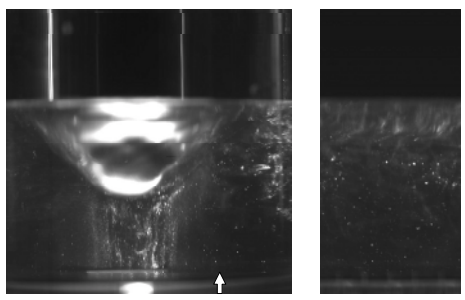

(a) (b)

Fig. 7. Visualized image obtained at Re = 0.62 × 10^5 (Ω = 330 rpm) (a) Snapshot and (b) temporally expanded images made by extracting line images, which have 1 pixel in width, snapshot location, r / R = 0.58. The time length of the temporally expanded image is 0.2 sec. The white arrow drawn in the snapshot indicates the extraction line of the line image.

Temporal variation of the flow pattern is investigated for three stages in the process of the switching phenomenon on the free surface; (A) deforming from axisymmetric to nonaxisymmetric, (B) detaching from the bottom and (C) reverting to axisymmetric and reattaching to the bottom (see Fig. 5).

Figure 8 shows the first stage of the switching, i.e., deformation of the free surface. Figure 8(a) is a snapshot extracted from the movie. Similar flow pattern shown in Fig. 3(c) can be observed. In Fig. 8, the deformation just starts to take place, from the axisymmetric to the nonaxisymmetric shape. Figures 8(b) and (c) show the temporally expanded images made by extracting line images from each snapshot at r /R = 0.58 and 0.86, respectively. The width of the line images is 1 pixel and the time length of the expanded image is 1 sec. Growth of the surface deformation is observed in Fig. 8(b). High brightness area, which expresses the edge of the deformed free surface, periodically appears in the bottom half of the figure. This becomes clearer with respect to time. The rotating speed of the humps on the free surface estimated from the image is 180 rpm and is around 23 % of the rotating speed of the disk, 770 rpm. The deformation of the free surface affects less the flow pattern near the free surface at this stage and there is no typical distribution of the brightness. The meridional circulation near the side wall is maintained but there is fluctuation of the circulation which has the same period of the rotating humps appearing in Fig. 8(b).

The flow in the second stage of the switching where the free surface detaches from the bottom is also explained in Fig. 9. Figure 9(a) is a snapshot of the flow extracted form the movie. The free surface in the snapshot assumes the nonaxisymmetric shape and has detached from the bottom. The flow near the center is well disturbed and there is no typical pattern indicating the local circulation region. Figures 9(b) and (c) are the temporally expanded images extracted from the movie, where the positions of the extraction are the same as in Figs. 8(b) and (c), respectively. The position of the extraction in the Fig. 9(b), r / R = 0.58, is close to the bottom of the rotating humps. The image reproduces well the detaching free surface with respect to time. The period of the appearing humps in the image is the same as that in the deformation process shown in the Fig. 8(b), around 180 rpm. The flow near the free surface is disturbed as expressed by the complex distribution of the brightness between the humps. The turbulence grows as the free surface detaching from the bottom. The flow disturbance caused by the humps of the free surface almost reaches the side wall as shown in Fig. 9(c). The flow is disturbed even in the bottom half of the cylinder. These variations shown in the temporally expanded images indicate that the flow becomes wholly turbulent during the process of the free surface detaching from the bottom. The turbulent flow is maintained while the free surface is kept above the bottom with the nonaxisymmetric shape.

Three snapshots in Fig. 10 show the flow at each time in the process at which the free surface assumes the axisymmetric shape again and then it reattaches to the bottom. The free surface in Fig. 9(a) has assumed the nonaxisymmetric shape, thus the flow is still wholly turbulent. The free surface descends to the bottom while reverting to its axisymmetric shape; the flow becomes laminar and the local circulation region reemerges near the center of the cylinder (Fig. 10(b)). The local circulation region expands in the radial direction just before the free surface attaches to the bottom (Fig. 10(c)). A temporally expanded image made of the horizontal line images near the disk represents the whole of the process (Fig. 10(d)), the vertical position of the extraction is z / H = 0.07 and the time length of the image is 3.07 sec. At the beginning of the image, there is a periodic

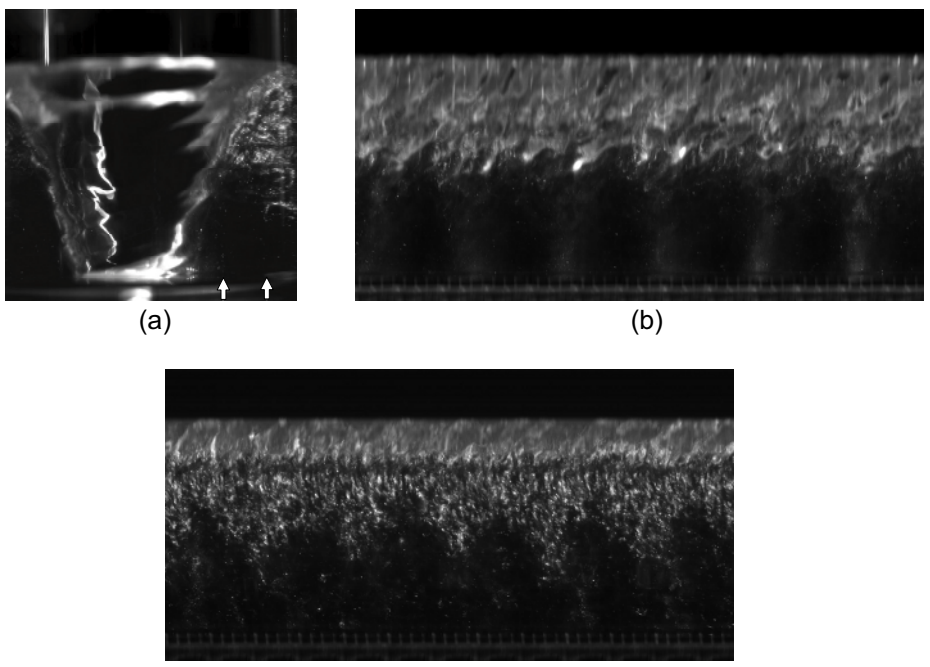

(a) (b)

(c)

Fig. 8. Visualized image obtained at Re = 1.46 $\times$ 10^5 (Ω = 770 rpm). The free surface is in the deformation process from symmetric to the nonaxisymmetric form, (a) Snapshot, (b) and (c) temporally expanded images made by extracting line images, which have 1 pixel in width, snapshot locations, r / R = 0.58 and 0.86, respectively. The time length of the images is 1 sec. The white arrows drawn in the snapshot indicate the extraction lines of the line image.

fluctuation of the brightness which corresponds to the movement of the humps. The fluctuation decreases with respect to time, but the asymmetry of the flow remains until the free surface completely attaches to the bottom (as in Fig. 8(a)). As explained in the introduction, the free surface sometimes assumes a nonaxisymmetric shape on the way to the bottom. In this case, the flow becomes turbulent and the free surface ascends again as the process shown in Fig. 9.

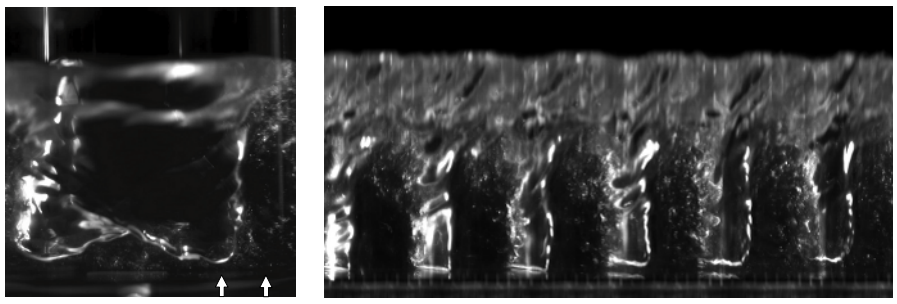

Fig. 9. Visualized image obtained at $Re = 1.46 \times 10^5$ (Ω = 770 rpm). The free surface is in the process of rising from the bottom, (a) Snapshot, (b) and (c) temporally expanded images made by extracting line images, which have 1 pixel in width, snapshot location, $r / R = 0.58$ and 0.86, respectively. The time length is 1 sec. The white arrows drawn in the snapshot indicates the extraction lines of the line image.

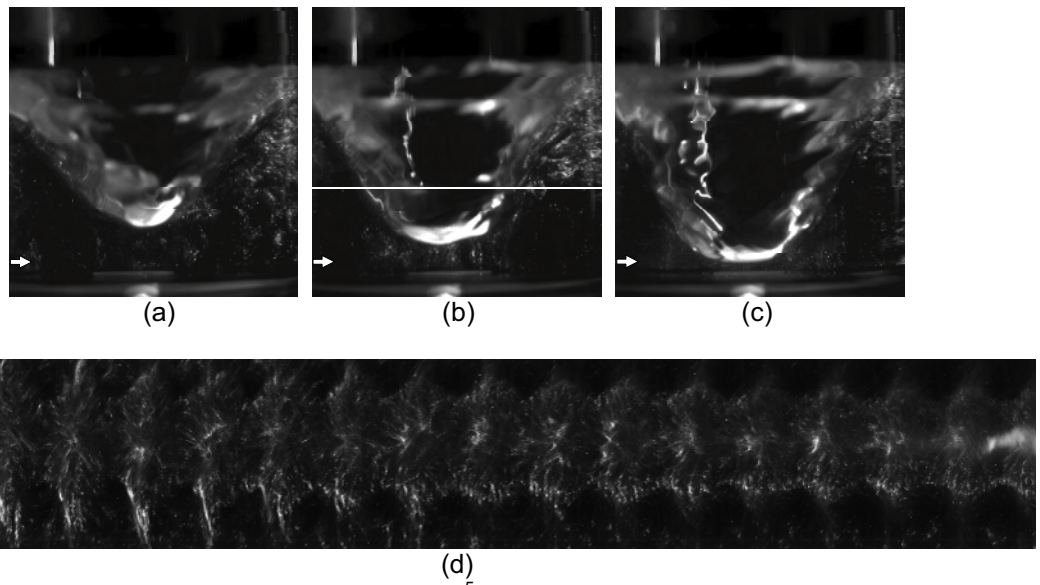

Fig. 10. Visualized image obtained at $Re = 1.46 \times 10^5$ (Ω = 770 rpm). The free surface is in the process of reattaching to the bottom, (a)(b)(c) Snapshots at each time, (d) temporally expanded image made by extracting line images from each snapshot at $z / H = 0.07$, where the time length is 3.07 sec. The white arrow drawn in the snapshot indicates the extraction line of the line image.

4. Conclusion

The rotating flow under the large-deformed free surface in the cylindrical vessel was investigated. This was done to clarify the relationship between the deformation of the free surface and the transition of the flow in the switching phenomenon process. In this phenomenon, the free surface changes from an axisymmetric shape to a nonaxisymmetric shape and vice versa with a repeating up-and-down motion. Flow pattern was visualized by means of anisotropic flakes, Kalliroscope, and the flow under the inverted-bell free surface in the visualized image was distinguished by three regions from the center to the side wall; the local circulation region, the rigid vortex region and the meridional circulation region. The images indicated that the rigid vortex is not stable near the center, hence circulation in the meridional direction occurs. The local circulation region disappears when the free surface attaches to the bottom at a high rotating speed. Snapshots of the flow and temporally expanded images extracted from movies of the flow clarify the flow transition under the switching phenomenon as follows. The flow near the free surface is still laminar even though the shape of the free surface changes to the nonaxisymmetric shape while the free surface attaches to the bottom. With free surface detaching from the bottom, the flow near the free surface is disturbed and finally, the flow becomes wholly turbulent. The free surface descends while changing its shape from the nonaxisymmetric shape to the parabolic-axisymmetric shape. On the way of this process, the flow changes from turbulent to laminar and the local circulation region reemerges at the center of the cylinder. The local circulation region is maintained until the free surface reattaches to the bottom. When the free surface assumes the nonaxisymmetric shape on the way of the descending process, the flow becomes turbulent and the free surface ascends again.

We are now measuring the turbulent intensity of the flow and has clarified that the turbulent intensity shows a jump at the critical Reynolds number for the surface switching. This is consistent with the present study, and the detail will be published in the forthcoming paper (Tasaka, et al., 2008). However, the effect of other parameters should be examined. In particular, the Froude number dominates the surface shape through the centrifugal force. Analyzing the surface in terms of such viewpoint is an interesting problem, but we would like to leave it as the topic of the future study. This phenomenon may have great application on mixing process, e.g. a control of mixing force with small changing on rotating speed of a rotor.

References

Jansson, T. R. N. et al., Polygons on a Rotating Fluids Surface, Phys. Rev. Lett., 96 (2006), 174502(1-4).
Lopez, J. M. et al., Symmetry breaking in free-surface cylinder flows, J. Fluid Mech., 502 (2004), 99-126.
Park, K., Grawford, G. L. and Donnelly, R. J., Determination of transition in Couette flow in finite geometries, Phys. Rev. Lett., 47 (1981), 1448-1450.
Poncet, S. and Chauve, M. P., Shear-layer instability in a rotating system, J. Flow Visualization & Image Proc., 14-1 (2007), 85-105.
Reed, H. L. and Saric, W. S., Stability of three-dimensional boundary layers, Ann. Rev. Fluid Mech., 21 (1989), 235-284.
Suzuki, T., Iima, M. and Hayase, Y., Surface switching of rotating fluid in a cylinder, Phys. Fluids, 18 (2006), 101701(1-4).
Tasaka, Y., Iima, M. and Ito, K., Flow transition in rotating flow relating with surface switching, IoP, J. Phys: Conference Series (accepted).
Thoroddsen, S. T. and Bauer, J. M., Qualitative flow visualization using colored lights and reflective flakes, Phys. Fluids, 11-7 (1999), 1702-1704.
Vatistas, G. H., A note on liquid vortex sloshing and Kelvin's equilibria, J. Fluid Mech., 217 (1990), 241-248.

Acknowledgement

A part of this work is supported by Grant-Aided Research for Science of the Japanese Ministry of Education & Science: No.18760116. The authors express thanks for this support.

Appendix

We estimate the radius of the rigid vortex observed in Fig. 3(b) under the assumption that observed flow in the vessel as Rankine's combined vortex which is combination of a rigid vortex region where the vorticity ω is a constant and a free vortex region where the $\omega = 0$ in an infinite fluid layer. We do not consider the effect of the lateral wall for simplicity. Figure A shows the position of the free surface determined by observing Fig. 3(b); (a) wide range ($-0.456 \leq r/R \leq 0.817$) and (b) narrow range (–0.199

$\leq r/\mathrm{R} \leq 0.208$) corresponding to the local circulation region. The extracted free surface has parabolic shape near the center and has an inflection point around $r/\mathrm{R} = 0.5$, which is close to the interface between the rigid vortex region and the meridional circulation region determined in Fig. 3(b). The solid and the broken lines represent a fitting function, $z/\mathrm{R} = A\,(r/\mathrm{R})^2 - Br/\mathrm{R} + C$ ($A = 1.2619$, $B = 0.0413$ and $C = 0.471$), estimated by the least square estimation on the data in the range of the rigid body region, $-0.456 \leq r/\mathrm{R} \leq 0.492$. The broken line in Fig. A(a) represents the outer bound of the estimation region. The white arrows in the photographs attached to the top of the figures indicate the range of the extraction. There is a systematic deviation from the fitting curve at the narrow range due to the influence of the local circulation. By using the estimated function, the height of the free surface, z, can be expressed as

$$z(r) = \begin{cases} \dfrac{\omega^2}{8g} r^2 + C\mathrm{R} & (r < a) \\ -\dfrac{\omega^2 a^4}{8gr^2} + \dfrac{\omega^2 a^2}{4g} + C\mathrm{R} & (a < r < \mathrm{R}) \end{cases} \tag{1}$$

where a expresses the radius of the rigid vortex (nonaxisymmetric component B is neglected here). Comparing the estimated function and equation (1) derives vorticity of the rigid vortex, $\omega = (8gA/\mathrm{R})^{1/2} = 48.27$ rad/s. Hence the rotating speed, $\omega/2$, becomes 230.48 rpm, around 70 % of the disk rotation Ω, 328 rpm. By integrating equation (1) at each range, the volume of the working fluid in the vessel, V, is determined as

$$V = \frac{\pi A}{2\mathrm{R}} a^4 + \frac{2\pi A}{\mathrm{R}} a^2 \left(a^2 \log \frac{a}{\mathrm{R}} + \mathrm{R}^2 - a^2 \right) + \pi C \mathrm{R}^3 . \tag{2}$$

The volume given from the size of the apparatus is $V/\mathrm{R}^3 = \Gamma\pi$ ($= 0.941\pi$), hence $a/\mathrm{R} = 0.570$ is obtained from equation (2). This value agrees well with the range of the rigid vortex in the observation, $a/\mathrm{R} \sim 0.5$. This calculation confirmed that the flow is almost laminar.

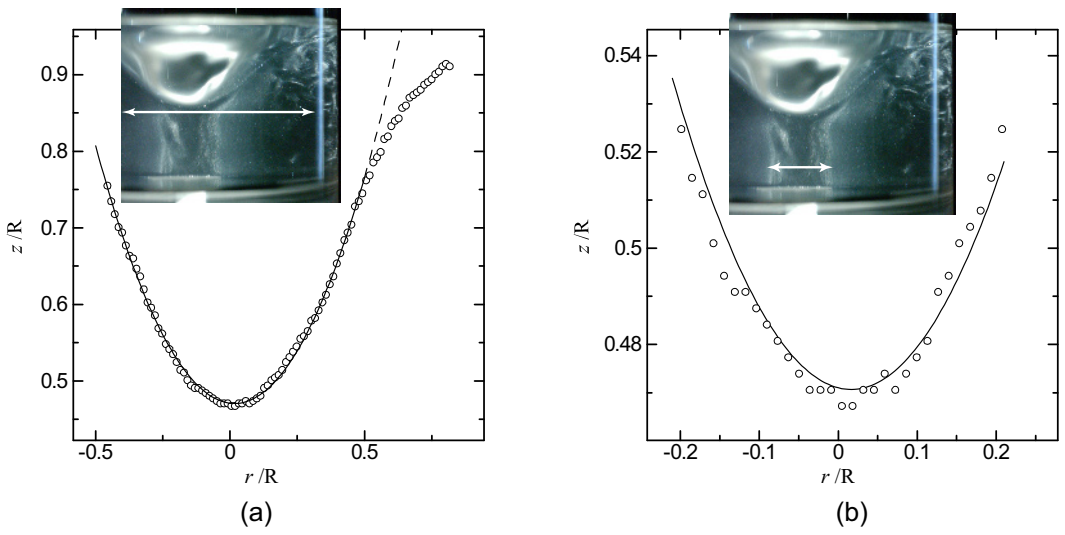

Fig. A. Position of the free surface obtained from Fig. 3(b); (a) wide range ($-0.456 \leq r/\mathrm{R} \leq 0.817$) and (b) narrow range ($-0.199 \leq r/\mathrm{R} \leq 0.208$) corresponding to an area of local circulation observed in the photograph. Solid and broken lines represent a fitting function estimated by the least square estimation on the data in the range of the rigid body region. The broken line means the outer bound of the estimation range. The white arrows in the photographs indicate the range of the extraction.

Author Profile

Yuji Tasaka: He received his M. Eng. in Mechanical Engineering in 2002 from Hokkaido University. He also received his Ph.D. in Mechanical Engineering in 2005 from the same university. He worked in the Graduate School of Engineering, Hokkaido University as a research associate. He is an assistant professor since 2006. His research interests are ultrasonic measurement of liquid metal flow, especially thermal convection, flow instability and transition processes from laminar flow to turbulent flow.

Kentaro Ito: He received his M.Sc. in Mathematics in 2005 from Hokkaido University. He is a Ph.D student in the Graduate School of Science, Hokkaido University since 2005. His research interests are dynamical systems, coupled oscillator systems, and bifurcation theory.

Makoto Iima: He received his M.Sc. degree in 1995 from Kyoto University. He also received his Ph.D. in fluid mechanics in 1998 from the same university. He worked in Research Institute for Electronic Sciences, Hokkaido University as a research associate, and currently he is an assistant professor since 1999. His research interests include turbulent phenomena, biofluid mechanics, and nonlinear systems.